Taylor & Francis
Taylor & Francis Group

Journal of Adhesion Science and Technology

ISSN: (Print) (Online) Journal homepage: https://www.tandfonline.com/loi/tast20

Self-assembled monolayers of novel imidazole derivative on copper surface for anticorrosion protection in neutral medium

Periyasamy Durainatarajan, Mallaiah Prabakaran & Subbaratnam Ramesh

To cite this article: Periyasamy Durainatarajan, Mallaiah Prabakaran & Subbaratnam Ramesh (2021): Self-assembled monolayers of novel imidazole derivative on copper surface for anticorrosion protection in neutral medium, Journal of Adhesion Science and Technology, DOI: 10.1080/01694243.2021.1895571

To link to this article: https://doi.org/10.1080/01694243.2021.1895571

JOURNAL OF ADHESION SCIENCE AND TECHNOLOGY
https://doi.org/10.1080/01694243.2021.1895571

Self-assembled monolayers of novel imidazole derivative on copper surface for anticorrosion protection in neutral medium

Periyasamy Durainatarajan[a], Mallaiah Prabakaran[b] and Subbaratnam Ramesh[c]

[a]Jairams Arts and Science College, Karur, India; [b]Department of Chemistry, Erode Sengunthar Engineering College, Erode, India; [c]Department of Chemistry, The Gandhigram Rural Institute–Deemed to be University, Gandhigram, India

ABSTRACT
In this paper, we report the 1-(3-aminopropyl)-2-methyl-1-imidazole (APMI) as self-assembled monolayers (SAMs) on copper surface *via* self-assembly to improve anticorrosion properties. Surface structure and bonding, chemical compositions, wettability and morphology of APMI SAMs on the surface of copper have been investigated by various surface analyses including FT-IR spectroscopy, energy dispersive X-ray analysis (EDX), X-ray photoelectron spectroscopy (XPS), contact angle measurement (CA) and atomic force microscopy (AFM). FT-IR and XPS analysis show that the APMI molecules are successfully self-assembled on the copper surface, forming a compact protective monolayer. CA measurements revealed the hydrophobic nature of SAMs. The corrosion resistivity of APMI SAMs against corrosion in 3% NaCl solution were studied by Tafel polarization and cyclic voltammetry techniques coupled with scanning electron microscopy and the results show that formed APMI monolayer on copper could prevent the corrosion reaction at the copper-solution interface effectively. The adsorption and corrosion inhibition behaviour of APMI SAMs on Cu are also investigated by quantum chemical calculations. Further, the obtained results from the present inhibitor were compared with the existed inhibitors from the literature.

ARTICLE HISTORY
Received 16 May 2020
Revised 5 January 2021
Accepted 6 January 2021

KEYWORDS
Copper; anticorrosion; X-ray photoelectron spectroscopy; contact angle; quantum chemical calculations

1. Introduction

Copper (Cu) for its favorable properties including high electromigration resistance, high thermal and electrical conductivity, which make it an attractive wide range technological applicant in architecture, circuit components, circuit board, industrial equipment and power transmission lines for communications [1]. Fatefully, corrosion is one of the major issues encountered in the Cu materials when exposed to surrounding environments such as moisture and aqueous chloride solution [2–4]. To overcome

CONTACT Subbaratnam Ramesh ✉ drsramesh_56@yahoo.com Department of Chemistry, The Gandhigram Rural Institute – Deemed to be University, Gandhigram, Tamil Nadu 624302, India

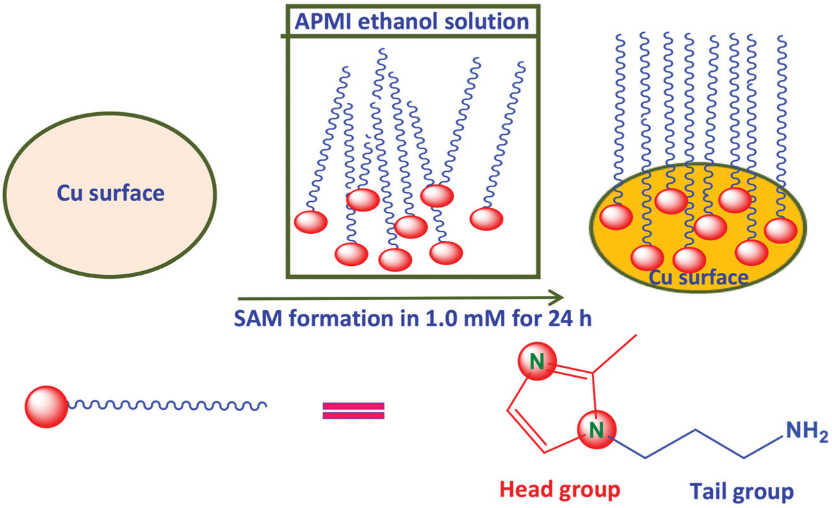

Scheme 1. Formation of APMI SAMs on copper surface.

this problem, a number of anti-corrosion strategies have been employed to protect corrosion of Cu. The surface modification with self-assembled monolayers (SAMs) is the effective method of protecting Cu surface against corrosion in chloride environment because of its simplicity, ease of fabrication, characterization, manipulation and the possibility of preparing monolayers with a high level of molecular arrangement [5,6]. So far, a number of researchers have reported the self-assembled monolayers on Cu surface for protection of Cu corrosion using various anticorrosion reagents such as alkanethiols [4,7], alkyl thiosulfate [8], aromatic thiol [5,9], phytic acid [10], Schiff bases [11], amino acid [12], Triazole [13,14], mercaptobenzimidazole [15,16], mercaptobenzoxazole [17,18] and mercaptobenzothiazole [19,20]. It has been documented in the literature that aromatic heterocyclic molecules bearing hetero donor atoms (N, S, O and P) with free electron pairs act as potential centers for binding with Cu surface and form an adherent protective film as a barrier to aggressive ions [21–23]. Fatefully, some of the commonly used heterocyclic molecules are toxic for living organisms and contaminate the environment as well as limit their usage in industrial applications. Nowadays research works are in progress to find new molecules with lower toxicity as corrosion inhibitors which has attracted the attention of numerous investigators. Azole compounds, such as imidazole and its derivatives have been reported as non-toxic molecules exhibiting high protection efficiency for metal corrosion in different solutions [24–28]. The family of imidazole-containing compounds is important not only for corrosion prevention also they display a variety of biological activities including antibacterial, antifungal, anticancer and anti-inflammatory agents [29–31]. The goal of this work is to investigate the inhibition performance of 1-(3-aminopropyl)-2-methyl-1-imidazole (APMI) derivative as corrosion inhibitor for Cu in 3% NaCl solution (Scheme 1). Besides, no attempt has been made so far to study the self-assembly of APMI on Cu against corrosion in 3% NaCl solution.

2. Experimental section

2.1. Materials

The APMI compound was supplied by Sigma-Aldrich and was used as received. All other materials employed in this investigation were of analytical grade (AR). APMI was dissolved in anhydrous ethanol to prepare 1.0–1.5 mM solutions. An aqueous solution of 3% NaCl was employed as the test solution. The working Cu electrode was prepared as follows: The surface of the electrode was sequentially polished with different metallographic grits paper (1/0–6/0) and then ultrasonically cleaned in ethanol for 10 min, followed by dried with a flow of nitrogen gas. They were directly self-assembled in different concentration of APMI ethanol solution for different assembly time for self-assembly. The assembled samples were brought out of APMI solution and rinsed thoroughly several times with ethanol followed by double distilled water to remove physically adsorbed particles on the electrode surface and then further used for surface characterization and electrochemical measurements.

2.2. Electrochemical methods

The electrochemical corrosion resistive behavior of bare Cu and SAMs coated Cu were tested in 3% NaCl solution by CHI electrochemical workstation (CHI 760 D, USA). The corrosion tests were carried out in a conventional three-electrode cell configuration including a bare Cu/Cu coated APMI electrode (geometrical size of 1 cm^2) as working electrode, platinum electrode as counter electrode and saturated calomel electrode (SCE) as reference electrode, respectively. Alternating current impedance measurements were carried out in open circuit potential (OCP) mode with an amplitude of 5 mV and scan ranging from 100,000 to 10 Hz. The obtained impedance results were analyzed and best fitted by ZSimpWin 3.2.1 impedance analysis software. The percentage of inhibition efficiency can be measured using the charge transfer resistance from the following equation:

$$IE(\%) = \frac{R'_{ct} - R_{ct}}{R'_{ct}} \times 100 , \tag{1}$$

where R'_{ct} and R_{ct} are the charge transfer resistance for the SAMs coated Cu and bare Cu, respectively. The Tafel polarization measurements were carried out at a sweep rate of 2 mV s^{-1} in the potential range from -250 to $+250$ mV vs. OCP. The inhibition efficiency can be evaluated using the corrosion current density as follows:

$$IE(\%) = \frac{i^0_{\mathrm{corr}} - i_{\mathrm{corr}}}{i^0_{\mathrm{corr}}} \times 100, \tag{2}$$

where i^0_{corr} and i_{corr} are the corrosion current densities of the bare and APMI SAMs modified electrodes, respectively. All the electrochemical analyses were conducted at room temperature. The optimum concentration and self-assembly time for the APMI SAMs formation on Cu surface has been determined through electrochemical impedance spectroscopy (EIS) studies.

2.3. Surface characterization

Fourier transform infrared (FTIR) spectra measurements were recorded on a JASCO 460 plus model spectrometer in the spectral range between 4000 and 400 cm^{-1} with a scan rate of 32 cm^{-1}. The IR spectrum of the pure APMI and APMI SAMs on Cu were obtained by KBr pellet technique. X-ray photoelectron spectroscopic (XPS) study was carried out using an Axis Ultra, Kratos Analytical with a monochromated Al Kα X-ray source (1486.6 eV). The morphology of bare Cu and SAMs modified Cu surfaces were analyzed with the aid of scanning electron microscopy (SEM, VEGA3 TESCAN) with 30 kV accelerating voltage while the elemental compositions on the Cu surfaces were analyzed by Energy dispersive X-ray analysis (EDX, Bruker Nano, Germany). The surface morphology at the nano to micro scale was further analyzed by contact mode atomic force microscopy (AFM, Nanosurf, Switzerland), which examines the nature of the protective film formed on the Cu surface from the three-dimensional (3 D) morphology. Contact angle analyses on Cu substrate surfaces were performed using the sessile drop method on contact angle goniometer (CA, 250-F1, Rame-Hart Instrument Co., USA) at room temperature and the volume of the water droplet is about 10 µl. Contact angle data collected by five different positions on each Cu substrate and then averaged to get reliable values.

3. Results and discussion

3.1. EIS studies

3.1.1. Effect of concentration

EIS is one of the most helpful and revealing technique for the corrosion determination of coated metals. Figure 1(a) shows the Nyquist impedance plots in 3% NaCl solution for the bare Cu and the Cu electrodes modified in different self-assembly concentrations of APMI solution for 24 h. As shown in Figure 1(a) (inset) the Nyquist spectrum of bare electrode in the NaCl environment displays two capacitive loops; a impedance loop in the high frequency portion which is not a perfect semicircle can be attributed to the dispersing effect as a result from defectiveness of the electrode surface and follows a Warburg impedance in the low frequency range. This could be due to the diffusion controlled reaction rather than charge transfer reaction [32].

The Nyquist impedance plots of Cu coated APMI electrodes are clearly different from that of bare electrode. For the Cu with APMI SAMs, the Warburg impedance disappeared at low frequency and the diameter of high frequency impedance arcs increases with increasing the concentration of APMI. This phenomenon is attributed to the formation of compact and ordered monolayer on the Cu surface, which inhibits the corrosion process at the interface of Cu metal and solution. Figure 1(b) depicts the Bode plots of (Φ vs. $\log f$ and $\log |Z|$ vs. $\log f$) bare electrode and APMI SAMs modified Cu electrodes, respectively. The Φ vs. $\log f$ curve shows that the phase angle of the APMI coated electrode in the low frequency is much higher than that of bare Cu and increases as the concentration of APMI increases, indicating the corrosion resistivity of Cu electrode improved at the higher inhibitor concentration. Bode diagram ($\log |Z|$ vs.

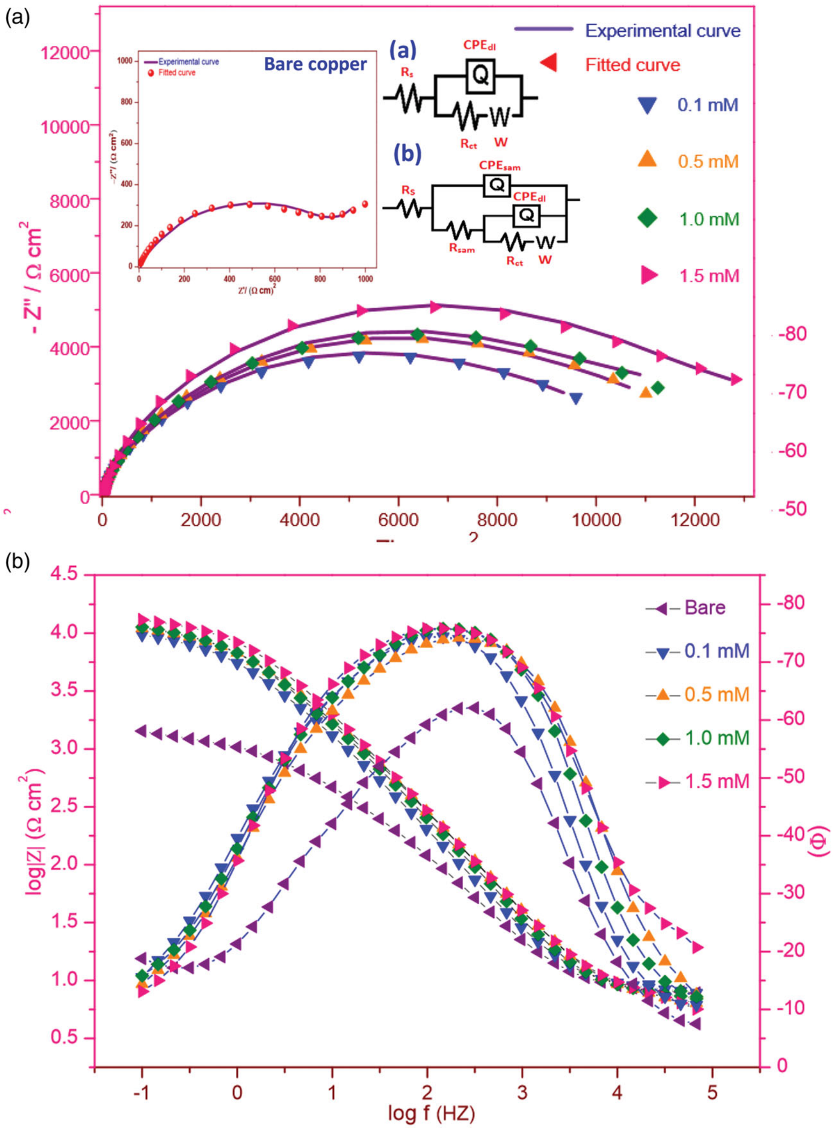

Figure 1. (a) Nyquist plot and (b) Bode – Phase angle plots in 3% NaCl for bare Cu (inset) and Cu electrodes self-assembled in different concentrations of APMI solution for 24 h (inset Figure 1(a): Equivalent circuit models used for fitting EIS experimental data of bare and APMI Cu).

log *f*) showed that the impedance amplitude increase in the presence of SAMs as compared to that of the bare Cu. The increase in amplitude at low frequency in Bode plot confirms the superior protection with rising APMI concentration. In EIS fit, constant phase element (CPE) is typically used to replace pure capacitor to substitute in the system of inhomogeneity [33]. The impedance of a CPE is expressed by the following equation.

$$Z_{CPE} = \frac{1}{Y_0 \; (j\omega)^{-n}} \tag{3}$$

Table 1. Nyquist impedance parameters obtained in 3% NaCl solution for the bare and Cu electrodes modified in different concentrations of APMI solution at self-assembly time for 24 h.

C (mM)	R_{ct} (Ω cm^2)	CPE_{dl} (μF cm^{-2})	n_1	R_{sam} (Ω cm^2)	CPE_{sam} (μF cm^{-2})	n_2	IE (%)
0	806	97.06	0.68	–	–	–	–
0.1	9758	50.67	0.47	2974	17.03	0.88	91.7
0.5	11,230	36.34	0.48	2828	12.61	0.87	92.8
1.0	12,330	36.17	0.50	2454	12.42	0.89	93.4
1.5	12,808	13.83	0.59	4640	9.15	0.85	93.7

where Y_0 is the magnitude, j is the imaginary root, ω is the angular frequency and n presents the CPE exponent which gives information about the degree of the surface inhomogeneity arising from surface roughness and surface defects. The equivalent circuits of experimental EIS results were analyzed and fitted by ZsimpWin impedance software and are displayed in Figure 1(a) (inset). R(Q(RW)) in Figure 1(a) is suitable for the Nyquist spectrum of the bare Cu while, in Figure 1(b), R(Q(R)(QR)) is suitable for the Nyquist spectrum of the APMI SAMs coated Cu electrode. The components of the equivalent circuit are listed in Table 1 which shows that the charge transfer resistance (R_{ct}), n values increase and capacitance values decreases as the concentration of APMI increases which might be due to the formation of a shielding barrier layer on the surface of the electrode by adsorption of APMI molecules. The increase of n values, with the concentration of the APMI, could be explained by the reduction in surface heterogeneity due to the accumulation of inhibitor molecules on the most active adsorption sites [34]. The decrease in capacitance values in presence of APMI demonstrated the decrease of the capacitive effects because the SAMs coating was apt to cover the charged surface [35]. By comparing the APMI SAMs coated Cu electrode with the bare Cu (Table 1), the values of R_{ct} increased remarkably. The value of R_{ct} increased from 9758 to 12,330 Ω cm^2 when the APMI self-assembly concentration was increased from 0.1 to 1.0 mM. Correspondingly, the inhibition efficiencies increase with the growing concentration of APMI and reach the optimum value of 93.4% at the concentration of 1.0 mM. However, when the assembly concentration reached to 1.5 mM, R_{ct} marginally increased to the value of 12,808 Ω cm^2 with the inhibition efficiency of 93.7%. The results suggest that the APMI monolayer formed on the Cu surface at the 1.0 mM concentration is more compact than other concentrations. The n value is increased from 0.47 to 0.50 and constant phase element of double layer (CPE_{dl}) values is decreased from 50.67 to 36.17 μF cm^{-2}. In addition, the resistance of the SAMs (R_{sam}) values increases and the constant phase element of SAM (CPE_{sam}) values decrease with raise in APMI concentration from 0.1 to 1.0 mM at 24 h. Therefore, 1.0 mM concentration of APMI is chosen as the optimum concentration to the formation of the SAMs on Cu surface.

3.1.2. Effect of self-assembly time

Figure 2 shows the Nyquist impedance and Bode plots in 3% NaCl solutions for the bare electrode and APMI modified Cu electrodes, which were self-assembled in 1.0 mM APMI solution at different immersion times. The corresponding impedance data were fitted by the equivalent circuit models shown in Figure 1(a) are listed in Table 2. The data of Table 2 reveal that for the Cu electrode self-assembled in APMI

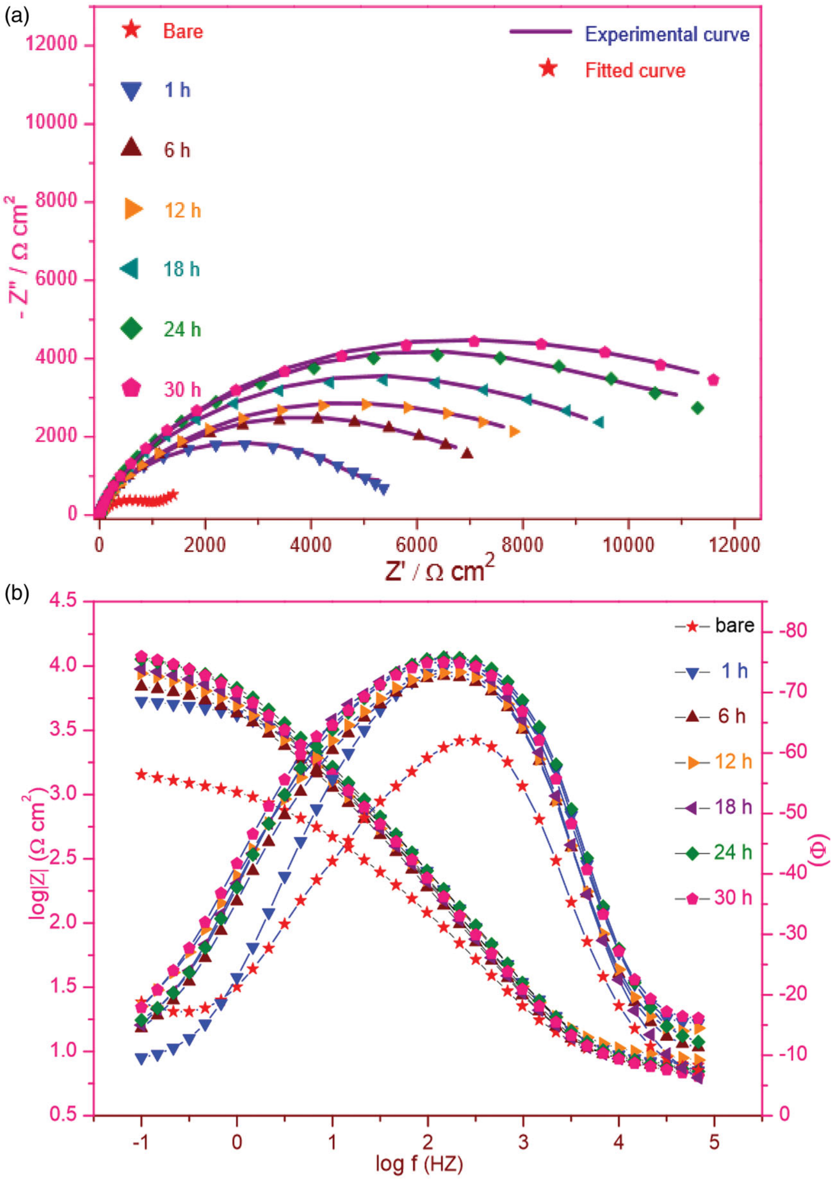

Figure 2. (a) Nyquist plot and (b) Bode – Phase angle plots in 3% NaCl for bare Cu and Cu modified electrodes self-assembled in 1.0 mM APMI solution at different self-assembled times.

solution for 1 h, R_{ct} value sharply raised to 3974 Ω cm^2 when compared to bare electrode (806 Ω cm^2) which is indicative of fast attachment of APMI molecules at the fresh Cu electrode surface. Further, the R_{ct} values increased from 6716 to 8724 Ω cm^2 with the Cu self-assembled in 6–12 h. When the assembly time was raised to 18 h, the R_{ct} reached to 11,080 Ω cm^2. While the assembly time increased to 24 and 30 h, the R_{ct} values were 12,330 and 12,620 Ω cm^2, respectively. However, the increase of R_{ct} values at assembling time of 24 and 30 h do not vary significantly, illustrating that the APMI molecules on the Cu surface have slowly rearranged to reach a compact and more

Table 2. Nyquist impedance parameters obtained in 3% NaCl solution for the bare and Cu electrode modified in 1.0 mM APMI solution at different self-assembly times.

t (h)	R_{ct} (Ω cm^2)	CPE_{dl} (μF cm^{-2})	n_1	R_{sam} (Ω cm^2)	CPE_{sam} (μF cm^{-2})	n_2	IE (%)
0	806	97.06	0.68	–	–	–	–
1	3974	83.62	0.42	2257	13.24	0.88	79.7
6	6716	60.95	0.49	2019	19.27	0.87	87.9
12	8724	59.83	0.49	1952	19.37	0.86	90.7
18	11,080	45.59	0.43	1893	14.77	0.89	92.7
24	12,330	36.17	0.50	2454	12.42	0.89	93.4
30	12,620	46.75	0.48	3735	16.25	0.87	93.6

ordered molecular arrangement after the self-assembling time for 24 h. It can be found in Table 2 that the inhibition efficiency of Cu with APMI is increased by increasing the time with optimum value, 93.4% at 24 h. With increasing self-assembly time both capacitance (CPE_{dl} and CPE_{sam}) values decrease and the charge resistance (R_{ct} and R_{sam}) values increased. From the EIS results, it is inferred that the optimum conditions for the formation of APMI SAMs on Cu surface are 1.0 mM concentration of APMI solution and self-assembly time of 24 h. These environments have been used for the construction of APMI SAMs on Cu surface throughout surface analysis and electrochemical studies.

3.2. Surface characterization of APMI SAMs

3.2.1. FT-IR spectroscopy

FT-IR is a simple and powerful analytical tool to investigate the chemical interactions between functional groups and the metal surface. Figure 3 presents the FT-IR spectra of pure APMI molecule and the APMI SAMs coated Cu substrate surface, respectively. The pure APMI spectrum showed stretching vibration modes namely: N–H stretching; 3429 cm^{-1}, CH_2 stretching vibration; 2962 cm^{-1}, C=N stretching; 1570 cm^{-1}, C–N stretching vibration; 1395 cm^{-1} (Figure 3(a)) [36].

On the other hand, in the spectrum of APMI SAMs coated Cu compared with pure APMI molecule; there is no appreciable band shift in the N-H stretching frequency region of the spectrum in Figure 3(a). However, APMI coated Cu shows the characteristic C = N stretching band shifting from 1570 to 1540 cm^{-1} and C–N stretching band from 1395 to 1380 cm^{-1} which are indicative of the chemical adsorption at the Cu surface had taken place through the N atoms in the imidazole ring (Figure 3(b)). These findings clearly demonstrate that the SAMs molecules have successfully self-assembled on the Cu substrate surface.

3.2.2. XPS analysis

In addition to the FT-IR measurement, XPS was performed to verify the formation of APMI SAMs on the Cu surface as well as mode of attachment to the Cu surface. XPS high resolution spectra for bare Cu (Cu 2p and O 1 s) and APMI coated Cu (Cu 2p, N 1 s, C 1 s and O 1 s) are shown in Figures 4 and 5, respectively. The XPS high resolution Cu 2p spectrum shown in Figure 4(a) exhibits the two peak components at 932.6 and 952.4 eV that are assigned to binding energy of Cu $2p_{3/2}$ and Cu $2p_{1/2}$, respectively, representing the presence of Cu (I) [37]. The intense peak at 531.5 eV in O 1 s

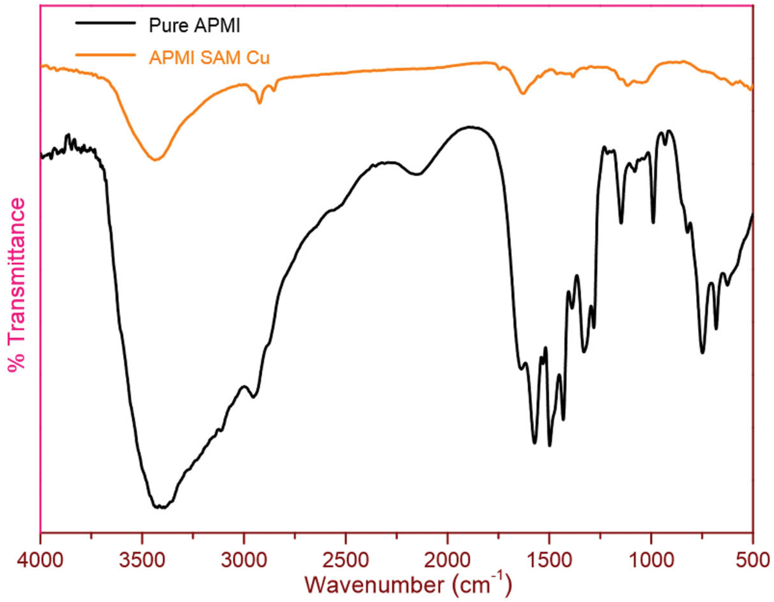

Figure 3. FT-IR spectra of (a) pure APMI molecule and (b) APMI SAM formed on Cu.

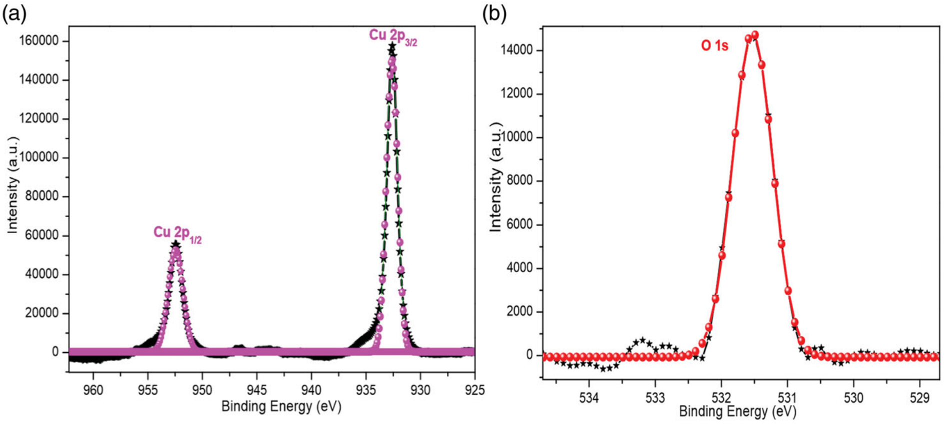

Figure 4. Curve fitting of XPS spectra of (a) Cu 2p (b) O 1 s of bare Cu.

spectrum is attributed to the Cu_2O which is formed during the time interval between abrading of the Cu surface and XPS analysis (Figure 4(b)) [38]. The APMI assembled Cu 2p spectrum shows the Cu $2p_{3/2}$ and Cu $2p_{1/2}$ observed with the binding energy 932.7 and 952.6 eV, respectively which arise due to the oxidation of Cu surface to Cu_2O during APMI SAMs modification (Figure 5(a)). Kamdem et al., reported in their studies that the Cu $2p_{3/2}$ peak at 935 eV and the presence of satellite peak indicate the presence of Cu (II) copper, while the peak around 933 eV and the absence of satellite peak indicate the presence of Cu (I) [39]. Therefore, it can be pointed out that the peak observed in our studies at 932.7 eV without any satellite peak is due to the presence of Cu (I) in the APMI Cu. The O1s peak detected at a binding energy of 531.5 eV is ascribed to the formation of Cu_2O on the electrode surface (Figure 5(b)). The existence

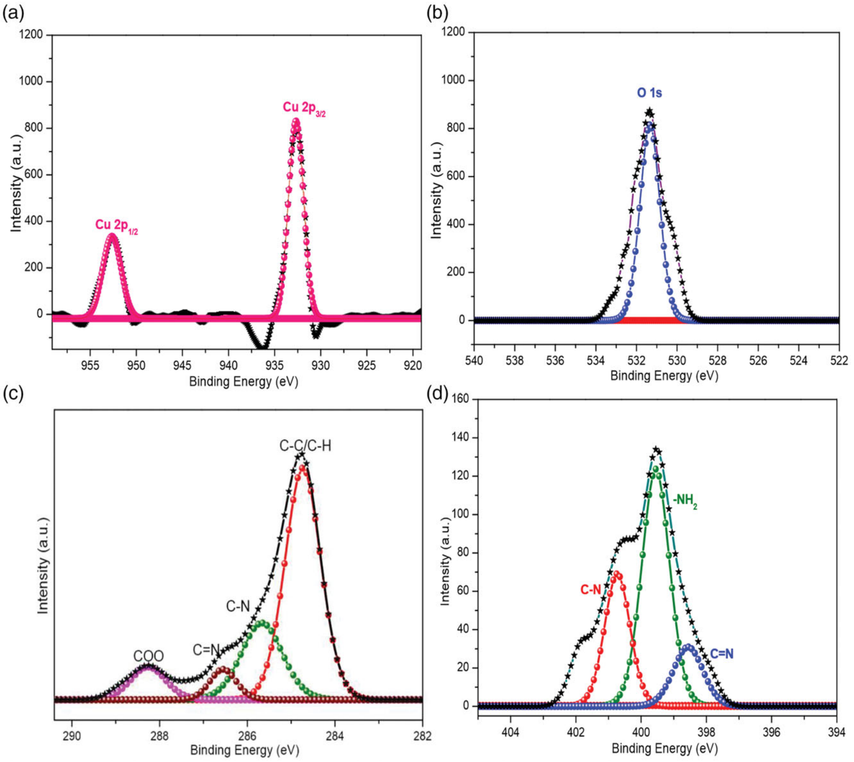

Figure 5. Curve fitting of XPS spectra of (a) Cu 2p (b) O 1 s (c) C 1 s (d) N 1 s of API SAM modified Cu.

of oxygen peak in the SAMs assembled Cu shows that oxygen dissolved in the APMI solution take part in the self-assembly process. The C 1 s spectrum has three peak components with the binding energies at 284.6, 285.5 and 286.2 eV, respectively. The peak component at high binding energy can be assigned to C–H/C–C and the other two peak component at lower binding energy can be attributed to C–N and C=N in the imidazole ring. Small peak at 288.1 eV is due to COO (Figure 5(c)). XPS high resolution N1s spectrum displays three components at 399.9, 398.7 and 400.2 eV that were ascribed to the neutral amino (–NH_2) group [40] and the C=N between carbon and pyridine nitrogen and C – N between carbon and pyrrole nitrogen [41], respectively (Figure 5(d)). The binding energy of the elemental nitrogen peak was reported at 398.0 eV in the literature [42]. The characteristic shift in N 1 s binding energy from elemental binding energy shows the APMI molecule is chemisorbed on cuprous surface through the N atoms in the imidazole ring. The results are in good agreement with those obtained by FT-IR spectroscopy studies.

3.2.3. SEM and EDX analysis

Surface modification on the Cu surface was examined by SEM and EDX techniques (Figure 6). As can be seen in the SEM micrograph (Figure 6(a)), polished Cu have uniform surface with few notches and lines on the surface which were introduced during polishing process. Correspondingly, the EDX analysis shows two elemental peaks at Cu

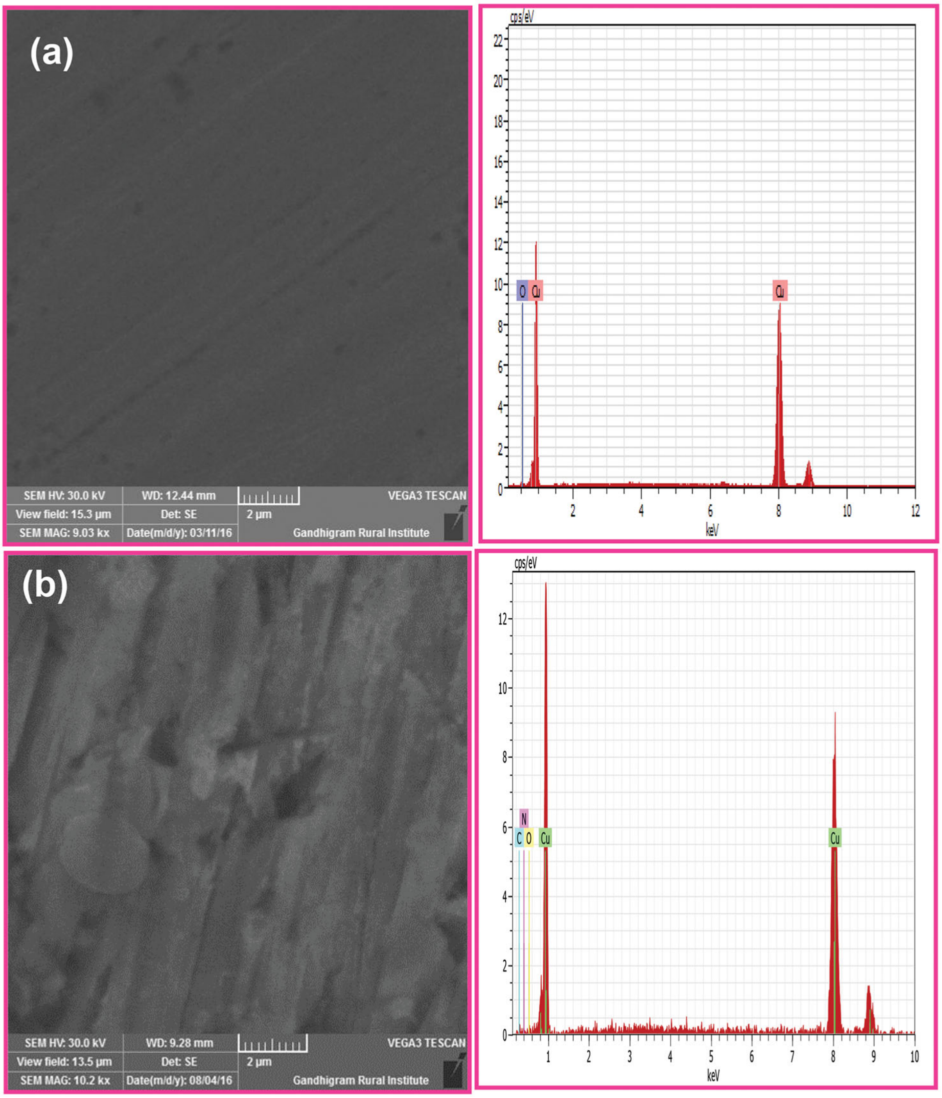

Figure 6. SEM micrographs and EDX spectra of (a) polished copper and (b) 2-MT SAM-covered copper.

at 0.93 and 8.05 keV and O at 0.53 keV, respectively. Whereas in the SEM micrograph of Figure 6(b), there is a dense protective film on the substrate associated with the presence of APMI and the notches are clearly also evident in the bare Cu. While EDX analysis shows new peaks for C at 0.28 keV, N at 0.39 keV along with Cu at 0.93 and 8.05 keV and O at 0.53 keV compared to bare one. The results are corroborating that the APMI SAMs was successfully accumulated over Cu surface.

3.2.4. Contact angle measurement

The wettability of the bare Cu and APMI SAMs coated surfaces were characterized by contact angle measurement. The photographic images of a drop of water on the bare and the APMI coated Cu surfaces are presented in Figure 7. It can

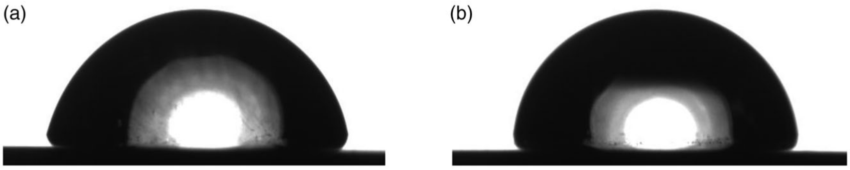

Figure 7. Contact angle images of (a) bare Cu surface and (b) APMI SAM coated Cu.

be found that the contact angle of the bare Cu was 77.5° (Figure 7(a)). On the other hand, for the Cu coated with APMI SAMs, the contact angle value clearly increased to 93.2° (Figure 7(b)) as compared to bare Cu. Thus, it has improved the contact angle for Cu substrate after the surface modification by APMI SAMs. It can be concluded that the APMI SAMs tailored onto the surface of the Cu and the increased hydrophobic properties of the Cu substrate can be ascribed to the polarity of APMI molecules.

3.2.5. AFM analysis

The morphology and surface roughness of Cu surface was detected by AFM technique. The 3 D AFM images (5 µm × 5 µm) of bare and APMI coated Cu substrates are given in Figure 8 and corresponding surface roughness parameters are tabulated in Table 3. As seen in Figure 8(a) the bare surface is covered with valleys and vertical lines due to the polishing process of Cu. The corresponding average surface roughness and root mean square roughness values are 13.217 and 16.699 nm. On the other hand, for the SAMs coated Cu surface was found to be relatively of uniform morphology with protecting layer and with the average surface roughness (S_a) and root mean square (S_q) values was observed to decrease significantly and reached 9.298 and 12.149 nm (Figure 8(b)). The significant reduction of S_a and S_q are ascribed to the formation of tight barrier film on the Cu, which shield the communication between SAMs Cu and chloride medium.

3.3. Evaluation of corrosion protection of copper

3.3.1. Tafel polarization studies

Figure 9 shows anodic and cathodic Tafel polarization curve of bare Cu and APMI coated Cu electrodes in 3% NaCl solution and corresponding tafel parameters tabulated in Table 4. The anodic Tafel polarization curve for bare Cu electrode in NaCl solution displays three different portions (Figure 9): Firstly, a Tafel region at lower over potentials which extending to the anodic peak current density (i_{peak}) owing to the oxidation of Cu (0) into Cu (I) [43].

$$\mathrm{Cu} \rightarrow \mathrm{Cu}^{+} + \mathrm{e}^{-} \tag{4}$$

Secondly, a region of decreasing anodic current until a minimum value (i_{min}) is reached due to formation of CuCl adsorbed layer [21] with anodic current hump centring around +0.023 V (SCE).

$$\mathrm{Cu} + \mathrm{Cl}^{-} \rightarrow \mathrm{CuCl} + \mathrm{e}^{-} \tag{5}$$

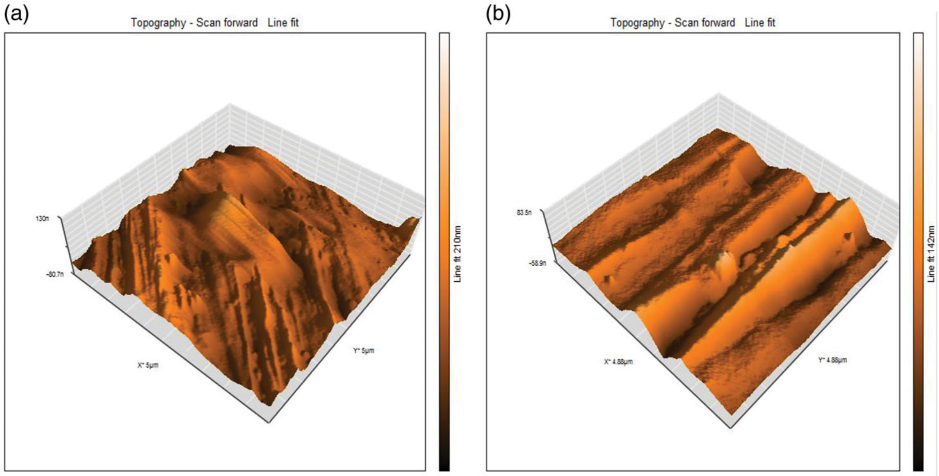

Figure 8. AFM images of (a) polished Cu and (b) APMI SAM coated Cu.

Table 3. Surface roughness parameters of bare Cu and APMI coated electrodes.

Electrodes	S_a (nm)	S_q (nm)
Bare Cu	13.217	16.699
APMI coated Cu	9.298	12.149

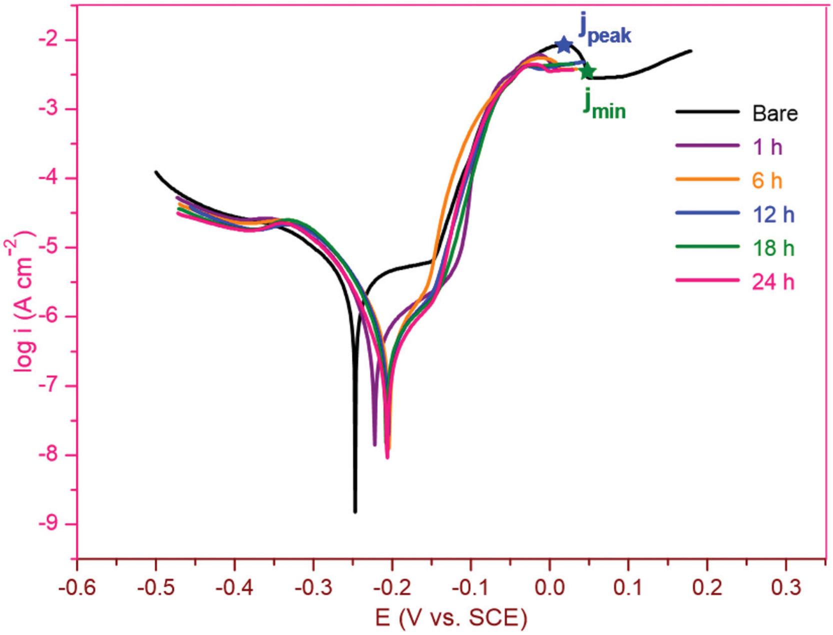

Figure 9. Tafel polarization curves in 3% NaCl environment for bare Cu and Cu coated electrodes self-assembled in 1.0 mM APMI solution for different time.

Table 4. Potentiodynamic polarization parameters obtained in 3% NaCl for the bare copper and copper electrode modified in 1.0 mM APMI solution at different self-assembly times.

t (h)	$-E_{corr}$ (mV/SCE)	I_{corr} (µA cm^{-2})	b_c (mV dec^{-1})	b_a (mV dec^{-1})	IE (%)
0	247	4.524	90	201	–
1	222	0.739	135	51	83.6
6	204	0.495	105	31	89.0
12	205	0.372	119	26	91.7
18	208	0.350	112	25	92.2
24	206	0.219	96	22	95.1

However, the formed CuCl layer is weakly adhered to the electrode surface and further attacked by Cl^- ions in the corrosive environment. Finally, the region of rapid increase in current density leading to limiting value, as a result of soluble $CuCl_2^-$ complex formation [44].

$$CuCl + Cl^- \rightarrow CuCl_2^- \quad (6)$$

Further, the soluble $CuCl_2^-$ species immediately diffused from the Cu electrode surface to the bulk solution [44].

$$CuCl_2^- \rightarrow Cu^{2+} + 2Cl^- + e^- \quad (7)$$

The APMI assembled electrode shows anodic peak current density decreases with a small current hump at −0.016 V (SCE) compared with bare Cu. It indicates that the APMI molecules are strongly adsorbed on the Cu surface which could decrease the oxidation of Cu(0) to Cu(I). The cathodic chemical reaction in NaCl solution is the reduction of the oxygen[45]:

$$O_2 + 4e^- + 2H_2O \rightarrow 4OH^- \quad (8)$$

As shown in Figure 9, in the APMI SAMs, the Tafel polarization curves move to the lower current densities, the corrosion potential (E_{corr}) are shifted to more positive potential direction and corrosion current (I_{corr}) decrease were observed in comparison to the bare Cu electrode. This effect is further enhanced by increasing the self-assembly time from 1 h to 24 h in 1.0 mM APMI concentration. Moreover, the direction of the E_{corr} is not uniform as it changes with changing concentrations of the APMI solution. This result suggests that the APMI SAMs coated Cu affect both the anodic dissolution and cathodic reduction process of the Cu electrode. The value of cathodic and anodic slopes (b_c and b_a) change with increasing the time are related to the decreases in both cathodic and anodic currents. Compared to the bare Cu substrate (Table 3), the E_{corr} and I_{corr} of the APMI Cu changed from −247 mV and 4.524 µA cm^{-2} to −206 mV and 0.219 µA cm^{-2}, respectively. It can also be observed that the inhibition efficiency increases from 83.6% up to 95.1% in 3% NaCl after the time increases from 1 to 24 h in 1.0 mM APMI. Corrosion inhibitor can be classified as an anodic- or cathodic-type based on the difference between E_{corr} values of Cu electrodes with and without SAMs that is larger than 85 mV or not [46]. In the present work, the E_{corr} with the SAMs shifts towards the anodic side and the maximum displacement is smaller than 85 mV

Table 5. Comparison of the inhibition efficiencies of different Cu inhibitors.

Inhibitor	Concentration (mM)	Medium	*IE* (%)	References
Benzotriazole (BTAH)	0.1–10	3% NaCl	75.4–89.3	Finsgar et al. [39]
Tetrazole (T)	1.0	0.1 M NaCl	53.5	Zucchi et al. [40]
5-Amino tetrazole (5-AT)			85.3	
Imidazole (IM)	0.1		49.8	Otmacic et al. [41]
4-Methyimidazole (4-MI)	0.1	3% NaCl	63.3	
1-Phenyl-4-methylimidazole (PI)	5.0		94.3	
Carbazole (CZ)	1.0		91.9	Wang et al. [42]
N-Vinyl carbazole (NVC)		0.5 M NaCl	93.4	
5-Mercapto-3-phenyl-1,3,4-thiadiazole-2-potassium (MPTT)	20.0	0.5 M NaCl	92.2	Chen et al. [24]
Methimazole (MT)	1.0	0.1 KCl	91.2	Pan et al. [43]
1-(3-Aminopropyl)-2-methyl-1-imidazole (APMI)	1.0	3% NaCl	95.1	This work

with respect to that without SAMs, which point out that the APMI SAMs Cu is a mixed inhibitor with mainly affecting the anodic dissolution of the Cu electrode. We have compared to our 1-APMI molecule with other Cu inhibitors studied such as benzotriazole (BTAH) [47], tetrazole (T) and 5-amino tetrazole (5-AT) [48], imidazole (IM), 4-methyimidazole (4-MI), and 1-phenyl-4-methylimidazole (PI) [49], carbazole (CZ) and N-vinyl carbazole (NVC) [50] 5-mercapto-3-phenyl-1,3,4-thiadiazole-2-potassium(MPTT) [32] and methimazole (MT) [51] in the neutral chloride solution and the comparisons are summarized in Table 5. From Table 5, protecting monolayer by APMI (inhibition efficiency reaching is 95.1%) in 3% NaCl solution seems to have better anticorrosive ability than the other Cu inhibitors. It should be mentioned that, for protecting the Cu, (BTAH, T, 5-AT, IM, 4-MI and PI) are added into the chloride solution and in other inhibitors (CZ, NVC, MPTT and MT) are coated at the Cu surface by self-assembly. From the above inhibitors, our APMI inhibitor has better inhibition efficiency as well as APMI solution could be recycled.

3.3.2. Cyclic voltammetric measurements

In order to further blocking efficiency of monolayer was studied by cyclic voltammetry (CV). Figure 10 shows the CV obtained for bare Cu electrode and APMI SAMs electrode after 1 h immersion in 3% NaCl solution. The Cu electrodes were scanned from negative to positive in the potential range of −0.6 to 0.6 V at a scan rate of 20 mV/s. As seen in Figure 10(a), the bare electrode in NaCl solution displays two anodic oxidation waves peaking at 0.19 V (labelled as I) and 0.35 V (SCE) (labelled as II) observed during the forward cycle which can be assigned to the oxidation of Cu(0) to CuCl adsorbed layer and further oxidation to soluble $CuCl_2^-$ complex formation on the Cu electrode surface [52–54] while corresponding a large cathodic reduction waves peak at −0.36 V (SCE) observed in the reverse cycle could be attributed to the reduction of the CuCl and soluble Cu complex to metallic Cu. By comparing with CV curve of bare Cu, APMI SAMs tailored Cu for the anodic and cathodic peak current domains are depressed significantly, along with the peak potential shift in both the forward and reverse sweep direction indicating that the APMI monolayers resist the chloride ions in the corrosive solution attacking the surface of the Cu electrode (Figure 10(b)). Thus, there is clear evidence that the APMI SAMs has been successfully self-assembled onto

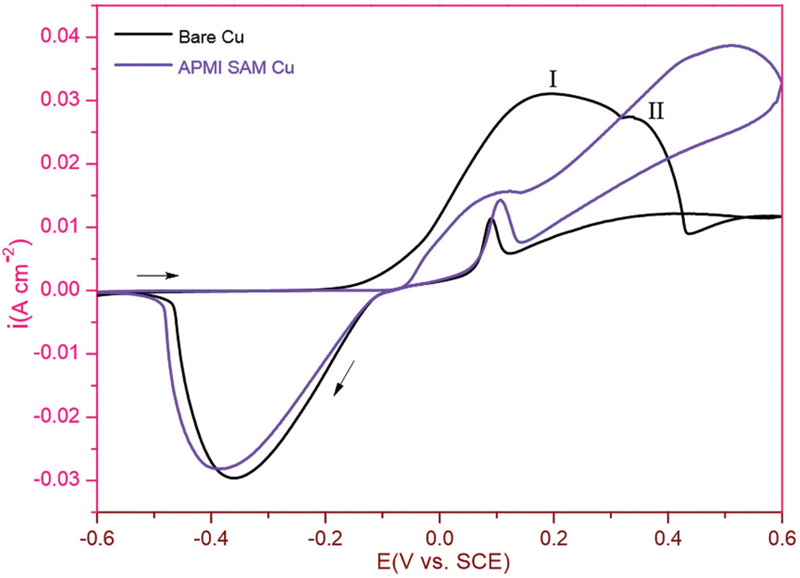

Figure 10. Cyclic voltammograms of (a) bare Cu and (b) APMI SAM coated copper electrodes in 3% NaCl solution.

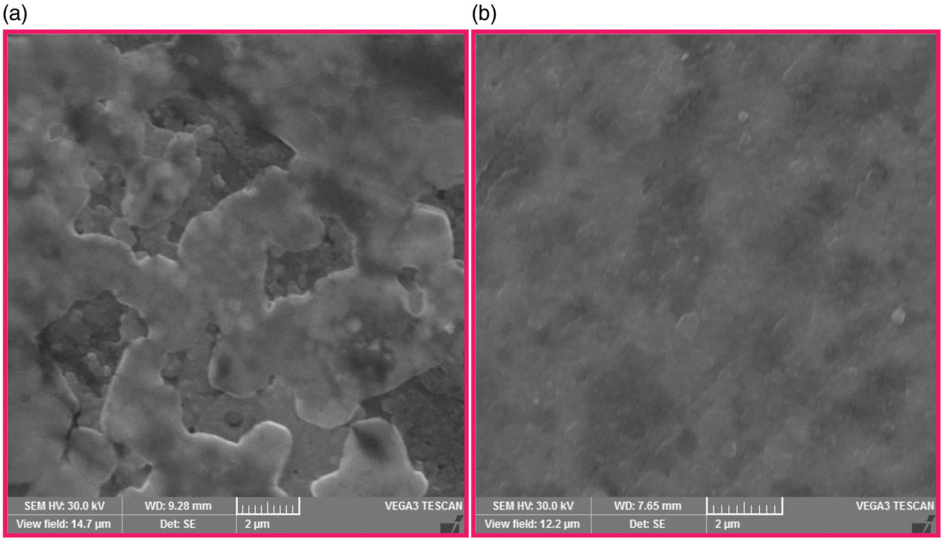

Figure 11. SEM micrographs of (a) bare Cu and (b) APMI SAM coated Cu after 3 days immersion in 3% NaCl solution.

the surface of the Cu electrode and the SAMs assembled Cu revealed a high anticorrosion property in 3% NaCl solution.

3.3.3. SEM analysis

To gain more insight into the surface morphological changes of Cu substrate in the absence and presence of APMI SAMs in 3% NaCl solutions they were examined by SEM analysis. Figure 11 shows the SEM micrographs obtained for bare

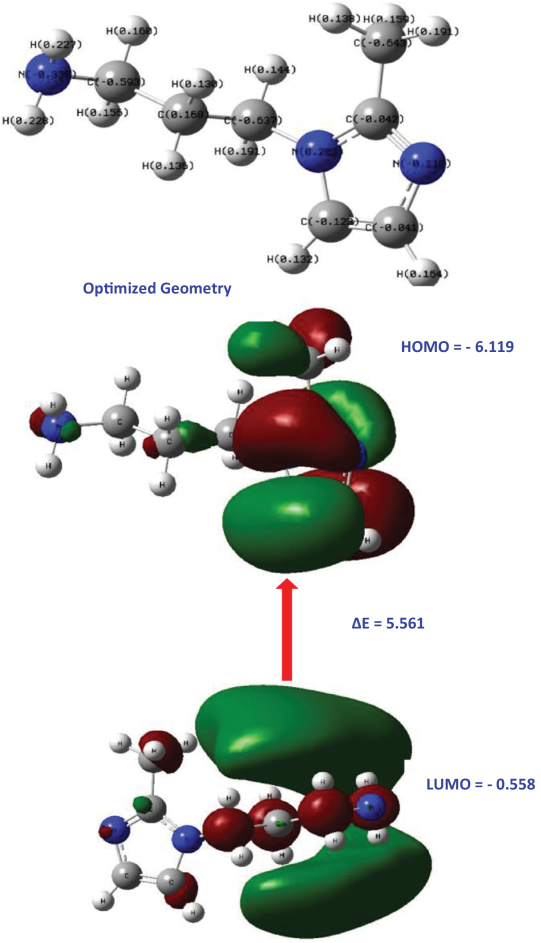

Figure 12. Optimized geometry and frontier molecular orbitals (HOMO and LUMO) of APMI inhibitor.

Cu and APMI SAMs coated Cu electrodes by immersing in 3% NaCl solution for 3 days. It can be observed from Figure 11(a) that in the absence of APMI, the surface is strongly damaged by the chloride environment; therefore, the surface is porous and with rough morphology. Whereas in the presence of SAMs (Figure 11(b)), the morphology of Cu was looks relatively smooth with no noticeable corrosion sign was detected. Observed results clearly show that SAMs coatings could effectively protect the Cu from corrosion in the aggressive environment and increase the corrosion resistance of Cu metal.

3.3.5. Quantum chemical calculations

The quantum chemical calculations are performed in order to elucidate the interactions between the inhibitor molecules and the Cu surface. Quantum chemical calculations are performed using DFT with the Becke's three parameter hybrid functional and the Lee-Yang-Parr correlation functional (B3LYP) with 6-311++G (d, p) basis set [46] for

Table 6. Calculated quantum chemical parameters for APMI inhibitor.

Inhibitor	E_{HOMO}	E_{LUMO}	ΔE (eV)	μ (D)	*IE* (%)
APMI	−6.119	−0.558	5.561	2.927	93.46

IE (%) value is calculated from EIS measurements.

all atoms with Gaussian 05 program. The optimized geometry, E_{HOMO} and E_{LUMO} of APMI molecule after optimization are presented in Figure 12 The relevant quantum chemical parameter's, namely, E_{HOMO}, E_{LUMO}, energy gap ($\Delta E = E_{LUMO} - E_{HOMO}$) and dipole moment (μ) are listed in Table 6. E_{HOMO} is related to the electron donating ability of the molecule. The high value of E_{HOMO} implies a tendency of the molecule to donate electrons to the unoccupied d-orbital of the Cu. On the other hand, E_{LUMO} represents the ability of the molecule to accept electrons, and the lower value of E_{LUMO} suggests more probability of the molecule to accept electrons [55,56]. The gap between E_{HOMO} and E_{LUMO} energy level of molecules is another important parameter that needs to be considered. The smaller the value of the $E_{LUMO} - E_{HOMO}$ energy gap (ΔE) for an inhibitor, the higher is the *IE* of that inhibitor [11,57]. Besides, the dipole moment (μ) is an index that can also be used for the prediction of a corrosion inhibition process. The *IE* has been reported to increase with decreasing dipole moment of the inhibitors [58]. As with energetic quantum parameters, some degree of irregularities appeared while dealing with dipole moment data in the interpretation of *IE* data, since the literature provides both positive [59] and negative [60] relationships between μ and *IE*. The present results show that APMI SAMs have a better protective effect for Cu corrosion and have lower ΔE values (5.561 eV), as compared to the reported literature. Besides, low values of the μ (2.927 D) could be attributed to the high symmetry of charge distribution in the APMI molecule, which may favour the accumulation of APMI molecules in the surface layer and therefore leads to the high *IE* [61]. This result is also supported by EIS measurements. From Figure 12, it is found that the electron cloud of HOMO is localized principally on the N atoms of imidazole ring, they can possibly be the active adsorption sites on Cu surface to form compact SAMs and inhibit Cu corrosion.

4. Conclusion

In this work, we have successfully employed an APMI inhibitor to form APMI SAMs on Cu to resist corrosion. The optimum concentration of APMI and optimum time for the self-assembly on Cu surface has been established using EIS studies. The surface characteristics of APMI coated Cu were characterized by FT-IR, XPS, EDX, CA and AFM analysis. FT-IR, XPS, EDX results show that APMI molecule can be easily chemisorbed onto the copper surface *via* self-assembly to achieve good anticorrosion effect. CA measurement displayed the hydrophobic nature of APMI SAM. The protection of APMI SAMs on Cu corrosion in 3% NaCl was investigated by Tafel polarization, CV and SEM analysis showing excellent inhibition properties for the corrosion of Cu surface in NaCl solution. The adsorption and corrosion inhibition behaviour of APMI SAMs were supported by quantum chemical calculations.

Disclosure statement

No potential conflict of interest was reported by the author(s).

References

[1] Núñez L, Reguera E, Corvo F, et al. Corrosion of copper in seawater and its aerosols in a tropical island. Corros Sci. 2005;47(2):461–484.

[2] Liang C, Wang P, Wu B, et al. Inhibition of copper corrosion by self-assembled monolayers of triazole derivative in chloride-containing solution. J Solid State Electrochem. 2010;14(8):1391–1399.

[3] Sung MM, Sung K, Kim CG, et al. Self-assembled monolayers of alkanethiols on oxidized copper surfaces. J Phys Chem B. 2000;104(10):2273–2277.

[4] Laibinis PE, Whitesides GM. Self-assembled monolayers of n-alkanethiolates on copper are barrier films that protect the metal against oxidation by air. J Am Chem Soc. 1992; 114(23):9022–9028.

[5] Behpour M, Mohammadi N. Investigation of inhibition properties of aromatic thiol self-assembled monolayer for corrosion protection. Corros Sci. 2012;65:331–339.

[6] Ruan CM, Bayer T, Meth S, et al. Creation and characterization of n-alkylthiol and n-alkylamine self-assembled monolayers on 316L stainless steel. Thin Solid Films. 2002; 419(1-2):95–104.

[7] Teo WK, Siow KS, Gao ZQ, et al. Corrosion protection of copper by a self-assembled monolayer of alkanethiol. J Electrochem Soc. 1997;144:55–64.

[8] Lusk AT, Jennings GK. Characterization of self-assembled monolayers formed from sodium S-alkyl thiosulfates on copper. Langmuir. 2001;17(25):7830–7836.

[9] Arslan E, Gurten AA, Gok HZ, et al. Electrochemical study of self-assembled aminothiol substituted phthalonitrile layers for corrosion protection of copper. Chem Select. 2017;2(27):8256–8261.

[10] Hao C, Yin RH, Wan ZY, et al. Electrochemical and photoelectrochemical study of the self-assembled monolayer phytic acid on cupronickel B30. Corros Sci. 2008;50(12): 3527–3533.

[11] Zhou Y, Xu S, Guo L, et al. Evaluating two new Schiff bases synthesized on the inhibition of corrosion of copper in NaCl solutions. RSC Adv. 2015;5(19):14804–14813.

[12] Zhang DQ, He XM, Cai QR, et al. Arginine self-assembled monolayers against copper corrosion and synergistic effect of iodide ion. J Appl Electrochem. 2009;39(8): 1193–1198.

[13] Vinothkumar K, Sethuraman MG. A robust method of enhancement of corrosion inhibitive ability of electrodeposited poly-3-amino-5-mercapto-1,2,4-triazole films over copper surface using graphene oxide. J Adhes Sci Technol. 2020;34(6):651–669.

[14] Hrimla M, Bahsis L, Boutouil A, et al. A combined computational and experimental study on the mild steel corrosion inhibition in hydrochloric acid by new multifunctional phosphonic acid containing 1,2,3-triazoles. J Adhes Sci Technol. 2020;34(16): 1741–1773.

[15] Chadwick D, Hashemi T. Electron spectroscopy of corrosion inhibitors: surface films formed by 2-mercaptobenzothiazole and 2-mercaptobenzimidazole on copper. Surf Sci. 1979;89(1-3):649–659.

[16] Wu X, Wiame F, Maurice V, et al. 2-mercaptobenzimidazole films formed at ultralow pressure on copper: adsorption, thermal stability and corrosion inhibition performance. Appl Surf Sci. 2020;527:146814–146814.

[17] Finšgar M, Kek Merl D. 2-Mercaptobenzoxazole as a copper corrosion inhibitor in chloride solution: electrochemistry, 3D-profilometry, and XPS surface analysis. Corros Sci. 2014;80:82–95.

[18] Yan CW, Lin HC, Cao CN. Investigation of inhibition of 2-mercaptobenzoxazole for copper corrosion. Electrochim Acta . 2000;45(17):2815–2821.

[19] Li J, Du CW, Liu ZY, et al. Inhibition film formed by 2-mercaptobenzothiazole on copper surface and its degradation mechanism in sodium chloride solution. Int J Electrochem Sci. 2016;11:10690–10705.

[20] Finšgar M, Kek Merl D. An electrochemical, long-term immersion, and XPS study of 2-mercaptobenzothiazole as a copper corrosion inhibitor in chloride solution. Corros Sci. 2014;83:164–175.

[21] Sherif EM. Effects of 2-amino-5-(ethylthio)-1, 3, 4-thiadiazole on copper corrosion as a corrosion inhibitor in 3% NaCl solutions. Appl Surf Sci. 2006;252(24):8615–8623.

[22] Antonijevic MM, Petrovic MB. Copper corrosion inhibitors. A review. Int J Electrochem Sci. 2008;3:1–28.

[23] Antonijevic MM, Milic SM, Petrovic MB, et al. Films formed on copper surface in chloride media in the presence of azoles. Corros Sci. 2009;51:1228–1237.

[24] Durainatarajan P, Prabakaran M, Ramesh S, et al. Self-assembly on copper surface by using imidazole derivative for corrosion protection. J Adhes Sci Technol. 2018;32(16): 1733–1749.

[25] Durainatarajan P, Prabakaran M, Ramesh S, et al. Surface protection of copper in 3% NaCl solution by using 1-(n-butyl)imidazole self-assembled monolayer. Mater Today Proc . 2018;5:16226–16236.

[26] Stupnišek-Lisac E, Gazivoda A, Madžarac M. Evaluation of non-toxic corrosion inhibitors for copper in sulphuric acid. Electrochim Acta. 2002;47(26):4189–4194.

[27] Appa Rao BV, Yakub Iqbal M, Sreedhar B. Electrochemical and surface analytical studies of the self-assembled monolayer of 5-methoxy-2-(octadecylthio) benzimidazole in corrosion protection of copper. Electrochim Acta. 2010;55(3):620–631.

[28] Appa Rao BV, Narsihma Reddy M. Formation, characterization and corrosion protection efficiency of self-assembled 1-octadecyl-1H-imidazole films on copper for corrosion protection. Arab J Chem. 2017;10:S3270–S3283.

[29] Molina P, Tárraga A, Otón F. Imidazole derivatives: a comprehensive survey of their recognition properties. Org Biomol Chem. 2012;10(9):1711–1724.

[30] Zhang L, Peng X-M, Damu GLV, et al. Comprehensive review in current developments of imidazole-based medicinal chemistry. Med Res Rev. 2014;34(2):340–437.

[31] Bhatnagar A, Sharma PK, Kumar N. A review on "imidazoles": their chemistry and pharmacological potentials. Int J Pharmtech Res. 2011;3:268–282.

[32] Chen W, Hong S, Li HB, et al. Protection of copper corrosion in 0.5 M NaCl solution by modification of 5-mercapto-3-phenyl-1, 3, 4-thiadiazole-2-thione potassium self-assembled monolayer. Corros Sci. 2012;61:53–62.

[33] Farsak M, Ongun Yüce A, Kardaş G. Anticorrosion effect of 4-amino-5-(4-pyridyl)-4H-1, 2, 4-triazole-3-thiol for mild steel in HCl solution. Chemselect. 2017;2(13): 3676–3682.

[34] Growcock FB, Jasinski RJ. Time-resolved impedance spectroscopy of mild steel in concentrated hydrochloric acid. J Electrochem Soc. 1989;136(8):2310–2314.

[35] Hong S, Chen W, Luo HQ, et al. Inhibition effect of 4-amino-antipyrine on the corrosion of copper in 3 wt.% NaCl solution. Corros Sci. 2012;57:270–278.

[36] Lalitha A, Ramesh S, Rajeswari S. Surface protection of copper in acid medium by azoles and surfactants. Electrochim Acta. 2005;51(1):47–55.

[37] Wang CT, Chen SH, Ma HY, et al. Study of the stability of self-assembled N-vinylcarbazole monolayers to protect copper against corrosion. J Serb Chem Soc. 2002;67(10): 685–696.

[38] Petkova G, Sokolova E, Raicheva S, et al. Corrosion inhibition of copper in near neutral aqueous solutions by gamma-pyrodiphenone. J Appl Electrochem. 1998;28(10): 1067–1071.

[39] Pascal KD, Zhang J, Alain A. Identification of cupric and cuprous copper in copper naphthenate-treated wood by X-ray photoelectron spectroscopy. Holzforschung. 2001; 55:16–20.

[40] Al-Khaldi TA, Lyon SB. The effect of interfacial chemistry on coating adhesion and performance: a mechanistic study using aminobutylphosphonic acid. Prog Org Coat. 2012;75(4):449–455.

[41] Liu X, Chen S, Tian F, et al. Studies of protection of iron corrosion by rosin imidazoline self-assembled monolayers. Surf Interface Anal. 2007;39(4):317–323.

[42] Beccaria AM, Bertolotto C. Inhibitory action of 3-trimethoxysilylpropanethiol-1 on copper corrosion in NaCl solutions. Electrochim Acta. 1997;42(9):1361–1371.

[43] Scendo M. Inhibition of copper corrosion in sodium nitrate solutions with nontoxic inhibitors. Corros Sci. 2008;50(6):1584–1592.

[44] Sherif EM, Park SM. Inhibition of copper corrosion in acidic pickling solutions by N-phenyl-1, 4-phenylenediamine. Electrochim Acta. 2006;51(22):4665–4673.

[45] Hu L, Zhang S, Li W, et al. Electrochemical and thermodynamic investigation of diniconazole and triadimefon as corrosion inhibitors for copper in synthetic seawater. Corros Sci. 2010;52(9):2891–2896.

[46] Li W, He Q, Zhang S, et al. Some new triazole derivatives as inhibitors for mild steel corrosion in acidic medium. J Appl Electrochem. 2008;38(3):289–295.

[47] Finsgar M, Lesar A, Kokalj A, et al. A comparative electrochemical and quantum chemical calculation study of BTAH and BTAOH as copper corrosion inhibitors in near neutral chloride solution. Electrochim Acta. 2008;53(28):8287–8297.

[48] Zucchi F, Trabanelli G, Fonsati M. Tetrazole derivatives as corrosion inhibitors for copper in chloride solutions. Corros Sci. 1996;38(11):2019–2029.

[49] Otmacic H, Stupnis ́ Ek-Lisac E. Protection of copper corrosion by carbazole and N-vinylcarbazole self-assembled films in NaCl solution. Electrochim Acta. 2003;48: 985–991.

[50] Wang CT, Chan SH, Ma HY, et al. Protection of copper corrosion by carbazole and N-vinylcarbazole self-assembled films in NaCl solutionJ. Appl Electrochem. 2003;33(2): 179–186.

[51] Pan YC, Wen Y, Xue LY, et al. Adsorption behavior of methimazole monolayers on a copper surface and its corrosion inhibition. J Phys Chem C. 2012;116(5):3532–3538.

[52] Li DG, Chen SH, Zhao SY, et al. The corrosion inhibition of the self-assembled Au, and Ag nanoparticles films on the surface of copper. Colloids Surf A. 2006;273(1–3): 16–23.

[53] Liao QQ, Yue ZW, Yang D, et al. Inhibition of copper corrosion in sodium chloride solution by the self-assembled monolayer of sodium diethyldithiocarbamate. Corros Sci. 2011;53(5):1999–2005.

[54] Lee YM, Chien YHC, Leung MK, et al. Surface protection of copper by self-assembly of novel poly (5-methylenebenzotriazol-N-yl). J Mater Chem A. 2013;1(11):3629–3638.

[55] Doner A, Solmaz R, Ozcan M, et al. Experimental and theoretical studies of thiazoles as corrosion inhibitors for mild steel in sulphuric acid solution. Corros Sci. 2011;53(9): 2902–2913.

[56] Tian H, Li W, Cao K, et al. Potent inhibition of copper corrosion in neutral chloride media by novel non-toxic thiadiazole derivatives. Corros Sci. 2013;73:281–291.

[57] Mobin M, Zehra S, Aslam R. L-Phenylalanine methyl ester hydrochloride as a green corrosion inhibitor for mild steel in hydrochloric acid solution and the effect of surfactant additive. RSC Adv. 2016;6(7):5890–5902.

[58] Gao G, Liang C. Electrochemical and DFT studies of β-amino-alcohols as corrosion inhibitors for brass. Electrochim Acta. 2007;52(13):4554–4559.

[59] Obot IB, Obi-Egbedi NO, Umoren SA. Antifungal drugs as corrosion inhibitors for aluminium in 0.1 M HCl. Corros Sci. 2009;51(8):1868–1875.

[60] Tang Y-M, Chen Y, Yang W-Z, et al. Electrochemical and theoretical studies of thienyl-substituted amino triazoles on corrosion inhibition of copper in 0.5 M H_2SO_4. J Appl Electrochem. 2008;38(11):1553–1559.

[61] Yadav DK, Maiti B, Quraishi MA. Electrochemical and quantum chemical studies of 3,4-dihydropyrimidin-2(1H)-ones as corrosion inhibitors for mild steel in hydrochloric acid solution. Corros Sci. 2010;52(11):3586–3598.